COPING WITH FLAP AND ACTUATOR DRIVING CONSTRAINTS IN ACTIVE ROTOR APPLICATIONS FOR VIBRATION REDUCTION

R. M. Morales*◇ and M. C. Turner*

* Dept. of Engineering, University of Leicester, University Rd., Leicester, UK, LE1 7RH, UK

◇Corresponding author: rmm23@le.ac.uk

Abstract

Among the various approaches to mitigate vibration, On-Blade Control (OBC) embeds actuation mechanisms on the blade in order to modify the vibratory loads at the source and achieve improved vibration reduction than conventional Higher Harmonic Control. Recent OBC studies have applied constrained optimisation methods to the design of vibration control algorithms to compensate against the effects of limited actuation and hence avoid significant performance degradation. These recent studies do not consider however constraints on the driving signals of the actuators. Such limitations can also have a significant and negative impact in the overall performance. For this, anti-windup control strategies are implemented to compensate against such actuator limitations. This work combines for the first time both actuator constraint handling methods for OBC applications and tested on a simplified model of a five-blade rotor with Active Trailing Edge Flaps. Performance results exhibit an improvement of almost a factor of 2 with respect to not using any constraint handling method.

1 INTRODUCTION

Current helicopter research and technology development efforts are devoted to mitigate the detrimental effects of primary vibrations originated on the main rotor since they contribute towards weak airworthiness, mechanical wearing and decreased flight comfort. Among the various approaches to mitigate vibrations on the main rotor, On-Blade Control (OBC) embeds actuation mechanisms on the blade in order to modify the vibratory loads at the source and hence attenuate their propagations across the helicopter fuselage. OBC devices offer the benefits of lower power consumption, increased bandwidth of operation, conceptual simplicity and lower weight penalty in comparison to pitch link actuated individual blade control devices [22, 3, 23]. In addition, OBC devices do not interfere with primary swashplate control commands in comparison to conventional Higher Harmonic Control (HHC) [11], hence having a reduced interference on the flight control system. Active trailing edge flaps (ATEFs) represents the most mature OBC device but it has not made it yet into the production stage despite successful flight tests [21] and wind tunnel campaigns [25]. Actively controlled flaps are embedded partially along the blade span as shown in Figure 1 and they can be found typically in single or dual configurations for increased control authority [1]. ATEFs can also be used in active rotor applications for the purpose of improving over additional fronts, such as noise [9], rotor performance [22] and dynamic stall characteristics [10].

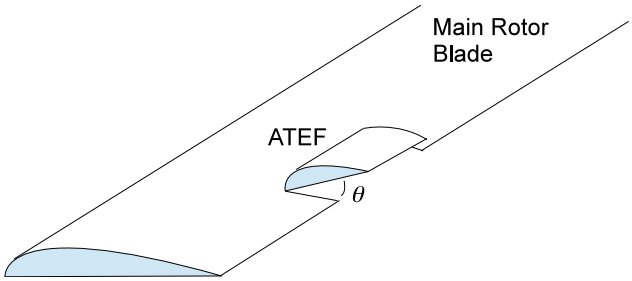

Figure 1: General schematic of an active trailing edge flap (ATEF) providing a deflection angle θ.

The general structure of OBC systems with ATEFs can be divided into two layers as shown in Figure 2. The outer loop, referred to as the *vibration control system*, processes shear and moment information in all three cartesian directions measured at the hub to produce a desired flapping signal $u(t)$ that needs to be conveyed in order to reduce vibrations. Such a reference flap signal is passed to an inner-loop control system (or *actuator control system*) and its objective

is to make the actual flap $\theta(t)$ as close as possible to the desired one $u(t)$ in the presence of centrifugal and Coriolis forces, wake interactions, actuator limitations, changes in RPM and actuator behaviour. Although recent research devotes most efforts to the design and stability analysis of the vibration control system [20], it is worth noting that the inner-loop actuator control system plays a crucial role in the success of the overall vibration reduction scheme.

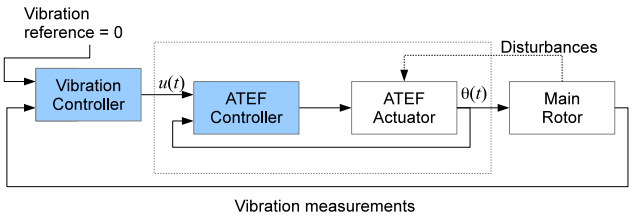

Figure 2: Overall control structure for vibration control using ATE actuators.

Vibrations at the rotor hub can be attributed to the complex wake structure, unsteady flow field and stall effects. A rotor with identical blades under identical loading and undergoing identical motion has hub forces and moments characterised by multiples of N/rev (N being the number of rotor blades), with 1/rev and N/rev harmonics being the more dominant at the non-rotating centre. There are other sources of vibrations such as engine transmission and aerodynamic forces on the fuselage [12] but it is the rotor influence, in particular the N/rev component, which is the main target of OBC vibration systems with ATEFs. The vibration controller is constructed from the assumption of a static linear relation between the Fourier coefficients of the most dominant harmonic and chosen harmonics of the actuation valid in steady forward-flight conditions. The modelling assumption extends to the existence of a baseline vibration, which is a non-zero vibration in the presence of zero actuation. Such a control strategy is derived from conventional HHC ideas [11] and they can be categorised as Adaptive Control [2], since the controller gains are updated from regular estimations of the open-loop process. Typically, the control law is constructed from the solution of an *unconstrained optimisation problem* [5], whereby a quadratic performance function, which encapsulates a weighted combination between vibration energy and control efforts, is minimised.

ATEF actuators can only deliver a limited range of deflection angles. Such actuator limitations are treated in a control theory framework as *output constraints*. If required, a pragmatic approach to deal with such constraints at the vibration control system level is to *scale* or *truncate* (clip) the control actions obtained from the solution of the unconstrained optimisation problem. Thus the requested reference flap signal is tolerated by the ATEF actuator control system. Another approach is to manipulate the weights in the performance function until the constraints are satisfied. Scaling and truncation can degrade significantly the achievable performance and such disadvantages have already been exposed by Friedmann and Padthe [9] for active rotor applications. In general, truncation changes the direction of the control actions leading potentially to very poor performance and therefore it should be avoided among all practices. Weight manipulation has the problem that the process of choosing a priori the input weight to meet the flapping constraints is not transparent and can be tedious. Iterative weight manipulation can be computationally expensive making it difficult for real implementations [9] and yet it does not guarantee that flap constraints are satisfied. In addition, overweighting control efforts can lead to very conservative performance. To overcome the issues exposed by scaling, truncation and overweighting, constrained optimisation techniques have been explored and shown to be a successful alternative [9]. Morales et al. [19] pay particular attention to *Quadratic Programming* (QP) [5] and shows its benefits over the the afore-mentioned techniques. Equivalent translations between time-domain flapping constraints and Fourier coefficients (frequency-domain) are not always possible in a QP framework and refined approximations might still be required in some scenarios. Such approximations should be taken into consideration carefully to avoid significant loss of optimal performance [15].

As mentioned earlier, the success of the overall control strategy relies also on the performance achieved by the actuator control system. ATEF actuators are constructed typically from piezoelectric materials. They exhibit lightly-damped second-order characteristics and their frequency behaviour has been shown to be sensitive to changes in RPM conditions [6, 14], with damping ratios and natural frequency values increasing with rotor speed. Feedback is therefore desired to reduce such a sensitivity. Large variations in the operating conditions, running under significant aerodynamic disturbances and operation at high frequencies can push the operation of the ATEF controller into saturation even with reference flap signals that fit within actuator capabilities [17]. For instance, the larger aerodynamics loads to be rejected by the actuator control loop, the larger actuator command signals are required to successfully reject such disturbances. Likewise, a large closed-loop bandwidth requires higher actuator driving efforts because the open-loop gain is typically lower at high frequencies [24]. Due to physical limitations of minimum and maximum (min-max) command efforts, the overall tracking performance can degrade significantly and in more extreme cases, the system

can become unstable [27, 16]. Actuator driving restrictions are treated in a control theory framework as *input constraints*. Actuator control systems with such saturation properties are more challenging to design due to the nonlinear nature of this behaviour [13]. To ameliorate the detrimental effects of input saturations at the actuator controller level, *anti-windup* control strategies [26, 29] have been implemented and proven successful by Morales and Turner [18] in preliminary applications of OBC.

Although control designs have been developed for each of the afore-mentioned limitations (flap and actuator driving constraints), they have not been implemented together. This is the main motivation of this work - to assess the benefits of implementing both constrained control techniques over implementing just one or none of them or in comparison to using more pragmatic approaches. The control ideas are implemented on a linearised model of a five-blade active rotor with dual flap configuration for the purpose of vibration reduction. The performance, which is expressed in terms of the average vibration reduction of the N/rev harmonic component, is shown to be improved by a factor of almost 2 with respect to the use of no constraint handling method.

The paper is structured as follows: both constrained control design strategies are introduced in the next two sections. The control strategies are applied to the simulation case study in Section 4. The paper concludes with some final remarks.

2 Constrained OBC via QP

By and large OBC laws are developed from Higher Harmonic Control ideas. For vibration reduction purposes, HHC is constructed from the assumption that the relation between selected Fourier (sine and cosine) coefficients of the actuator signal and output forces and moments [11] is linear. Such representation aims to capture up to some extent the quasi-steady rotor response in cruise flight conditions. Define a vector y_k as the output containing the harmonics of the loads and vibrations at the time instant indicated via the index k, with $t = k\Delta t$ and Δt representing the time gap between each implementation of the control actions. Likewise, define the input vector u_k containing the harmonics of a control input signal. The above assumption in the modelling of the rotor system is encapsulated in the following mathematical expression:

$$y_k = Tu_k + d \tag{1}$$

where d represents the harmonics of the baseline vibration, which is equivalent to y_k when the control inputs are zero ($u_k = 0$). Commonly, the matrix T is referred to as the *interaction matrix* or *sensitivity matrix* [20]. The above model is referred by Johnson [11] as the *global model* of helicopter response and can be rewritten as

$$y_k = y_0 + T(u_k - u_0) \tag{2}$$

u_0 represents the initial control input.

Control algorithms are based on the minimisation of a performance function J_k at the time index k, which is expressed in a quadratic form for mathematical convenience, and whereby a trade-off between vibration reduction and actuator efforts is specified:

$$u_k^\dagger = \arg\min_{u_k} \underbrace{y_k^T Q y_k + u_k^T R u_k}_{J_k} \tag{3}$$

Typically for vibration reduction, y_k contains the sine and cosine components of the N/rev hub loads and moments. The weight $Q = Q^T > 0$ is used to target specific vibration reduction among some of the vibration channels. Likewise, the weight $R = R^T > 0$ is used to specify actuator authority in the frequency domain. For instance, more weight can be associated to lower harmonics as the actuator control system is expected to perform better at such frequencies than at higher ones [18]. Often, both weights are diagonal and may be scaled differently if sensor measurements are provided in different units. A good starting point when designing the controller is to chose the same weight for all channels, which corresponds to $Q = R = I$, given that all vibration measurements as well as control signals are provided in the same units and actuators have enough bandwidth.

In the case where the optimisation problem is considered without actuator constraints, an analytic solution can be found by making

$$\frac{\partial J_k}{\partial u_k} = 0 \tag{4}$$

Solving for u_k provides the following analytical expression for the optimal control input

$$u_k^\dagger = -(T^T Q T + R)^{-1}(T^T Q)\underbrace{(y_0 - Tu_0)}_{d} \tag{5}$$

This is the classical expression for the HHC algorithm. There are many variants of the above algorithm, including adaptive forms. For more information refer to [2, 20] and [7].

The implementation of unconstrained control laws can lead to actuation signals which exceed actuator limits [9]. In order to better handle actuator constraints, it is recommended to instead use optimisation algorithms, which minimise the performance function given a feasible set of control input values. If the objective function is (convex) quadratic and the constraint functions are linear inequalities, the control

algorithm can be implemented as a *Quadratic Programming* [5]:

$$u^{\dagger\dagger} = \arg\min_{u_k} \underbrace{y_k^T Q y_k + u_k^T R u_k}_{J_k}$$

$$\text{(6)} \qquad \text{s.t.} \quad Hu_k \leq f$$

The above constrained optimisation problem can be equivalently written only in terms of the optimisation variable u_k for OBC systems with the use of (1) as:

$$u^{\dagger\dagger} = \arg\min_{u_k} \ \frac{1}{2} u_k^T (T^T Q T + R) u_k + u_k^T T^T Q d$$

$$\text{(7)} \quad \text{s.t.} \quad Hu_k \leq f$$

Note that the symbol $\leq$ indicate element-wise inequality. If the number of inequalities required to express the actuator constraints is p, then H and f have dimensions $p \times 2m$ and $p \times 1$, respectively. m is associated with the number of chosen harmonics to perform the control. A region of actuator signals is specified via the polyhedron $Hu_k \leq f$, which will be shown to be sufficient for active rotor applications.

2.1 Description of the constraint set

Flap constraints in the actuating device are expressed in the time domain as

$$\text{(8)} \qquad |u_i(t)| < \bar{u}, \forall i, \forall t$$

for a given $\bar{u} > 0$. The signal $u_i(t)$ is periodic and with selected harmonics to be manipulated

$$\text{(9)} \quad u_i(t) = \sum_{n=\underline{n}}^{\bar{n}} u_{i,c,n} \cos(n\Omega t) + u_{i,s,n} \sin(n\Omega t), \forall i, \forall t$$

The index triad $\{i, \{c, s\}, n\}$ is used to easily map the harmonic coefficients. The first index $i = \{1, ..., \bar{i}\}$ has been included to account for the fact that there can be more than one actuator on each blade. It is common to find two ATEFs with one actuator mounted in the *inboard* and the other on the *outboard* section of the blade to increase control power. The second index set $\{c, s\}$ are include to indicate the cosine and sine coefficients. The index $n = \{\underline{n}, \underline{n}+1, ..., \bar{n}\}$ denotes the frequency multiples at which the actuator operates. The number of harmonics selected for control are indicated by $m = \bar{n} - \underline{n} + 1$, with $0 < \underline{n} \leq \bar{n}$. Ω indicates the rotor speed in rad/s.

Translations of the time-domain constraint can be expressed in an equivalent form in terms of the Fourier coefficients as shown in [15]:

$$\text{(10)} \qquad \sum_{n=\underline{n}}^{\bar{n}} \sqrt{u_{i,c,n}^2 + u_{i,s,n}^2} \leq \bar{u}, \forall i$$

It is clear that the above set representation is nonlinear. It is then required to approximate the constraint set via linear inequalities so they can be incorporated in a QP framework. Typical implementations of constrained OBC via QP uses so-called box or infinity-norm constraints [9, 8]:

$$\text{(11)} \qquad |u_{i,c,n}|, |u_{i,s,n}| \leq \beta, \forall i, \forall n$$

In order to ensure that the original flap constraints are satisfied, we require that

$$\text{(12)} \qquad \beta = \frac{\bar{u}}{m\sqrt{2}}$$

It is clear then that box constraints can lead to conservative performance, especially when the dimension m is large [15].

In this work we will implement the QP using instead 1-norm constraint set representations as follows

$$\text{(13)} \qquad \sum_{n=\underline{n}}^{\bar{n}} |u_{i,c,n}| + |u_{i,s,n}| \leq \bar{u}, \forall i$$

The above approximation of the constraint set leads to less conservative results, as it will be shown later in the Simulation section. For more information about constraints descriptions for constrained OBC, refer to [15].

3 Anti-windup actuator control design

Actuator control systems consist typically of a standard feeback control structure in order to offer satisfactory tracking and disturbance rejection in the face of a changing operating environment. ATEFs are usually required to operate for a relatively small range of flap deflections, facing unpredictable and possibly significant air perturbations. Such exogenous effects can drive the operation of the actuator away from a desired operating condition and large command signals, which are beyond the acceptable limits of the actuator, could be induced. It is therefore adopted as a standard practice to saturate or limit the command signals within a certain interval to protect the actuating device. The introduction of such a limitation in the actuator closed loop can cause degradations such as sluggishness, highly oscillatory responses and in some more critical scenarios, instability (referred here as divergence of any of the signals in the control loop) when operating in high demanding conditions. The introduction of the limitation in the command signals is also known to have a negative impact on the robustness of the closed loop [16]. With some abuse in the terminology, the term *windup* is used to refer to the degradation in performance of the feedback control loop experienced in such operating conditions.

$$\min \ \gamma_{aw}$$

$$\text{such that} \begin{bmatrix} Q_{aw}A^T + AQ_{aw} + L^TB^T + BL & BU - L & 0 & Q_{aw}C + L^TD^T & L^T \\ \star & -2U & I & UD^T & U \\ \star & \star & -\gamma_{aw}I & 0 & -I \\ \star & \star & \star & -\gamma_{aw}W_p^{-1} & 0 \\ \star & \star & \star & \star & -\gamma_{aw}W_r^{-1} \end{bmatrix} < 0 \tag{14}$$

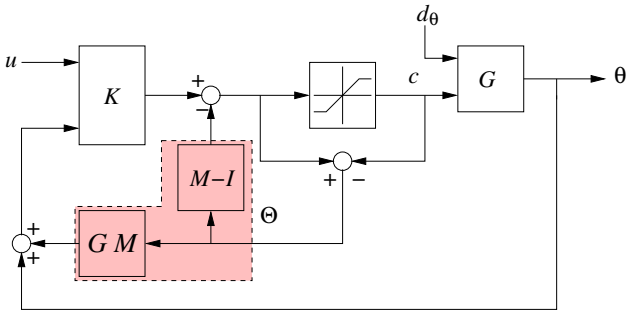

Figure 3: Anti-windup structure.

A common approach to deal with command signal saturation, is to augment the standard control system to preserve and emulate, whenever possible, the behaviour as if there were no constraints. Such attributes are known as *small signal preservation and unconstrained response recovery* and are at the core of the anti-windup philosophy [29]. Needless to say, a necessary condition for a successful anti-windup strategy based on this principle is that the performance achieved by the closed-loop in the absence of constraints is satisfactory. In addition, anti-windup elements are restricted to become active only when the system is sensed to be saturated.

For this particular study, the anti-windup design proposed by Turner et al. [27] has been considered due to its facility in the design and possibility to specify a desired trade-off between robustness and performance for saturated behaviour. This anti-windup architecture has its origins from the anti-windup scheme proposed by Weston and Postlethwaite [28]. The anti-windup scheme is depicted in Figure 3. In our case, the delivered deflections θ are assumed to be in the form $\theta = G(s)c + d_\theta$, with d_θ representing air disturbances, $G(s)$ the transfer function that models the open-loop behaviour of the actuating mechanism and c is the saturated command signal. $K(s)$ is the controller transfer function and it is assumed to be designed using linear control design techniques [24].

The anti-windup design is concerned with the choice of the LTI element $M(s)$, which in turn determines the form of the anti-windup compensator which is represented by the transfer function matrix

$$\Theta(s) = \begin{bmatrix} M(s) - I \\ G(s)M(s) \end{bmatrix} \tag{15}$$

with I representing the identity matrix. In the approach of [27], $M(s)$ is chosen as part of a coprime factorisation of the feedback portion of the actuator, $G(s) = N(s)M^{-1}(s)$ which enables the choice of $M(s)$ to be cast as a state-feedback design problem. The main idea behind the design of this anti-windup structure is to choose $M(s)$ so a performance function is optimised. The performance function consists of a weighted combination of two maps: one representing the effects of plant uncertainty (robustness) and the other the effects of saturation (performance).

The technical details of the anti-windup design are beyond the scope of this paper, but in essence the design of $M(s)$, and therefore the anti-windup compensator, can be achieved by solving a Linear Matrix Inequality optimisation problem [4]. More specifically, given a state a state-space realisation of the nominal behaviour of the actuator

$$\begin{aligned} G(s) &= C(sI - A)^{-1}B + D \\ &\sim \left[\begin{array}{c|c} A & B \\ \hline C & D \end{array}\right] \end{aligned}$$

then an anti-windup compensator which provides global asymptotic stability and, in some sense achieves "good" saturated performance can be designed from the solution of the LMI (14). In this LMI, the value of γ_{aw} represents in some sense the norm of the combined maps mentioned above and hence the lower its value the better the achieved performance of the anti-windup scheme in terms of unconstrained response recovery. The LMI problem in (14) is solved in terms of the variables $Q_{aw} > 0$, $U > 0$ and with diagonal structure, L and $\gamma_{aw} > 0$, where

$$F := LQ_{aw}^{-1} \tag{16}$$

The anti-windup element $\Theta(s)$ is finally obtained as

$$\Theta(s) \sim \left[\begin{array}{c|c} A + BF & B \\ \hline F & 0 \\ C + DF & D \end{array}\right] \tag{17}$$

4 SIMULATION EXAMPLE

4.1 The Rotor Model

In order to illustrate the ideas discussed in this report, simulations have been performed on a linearised

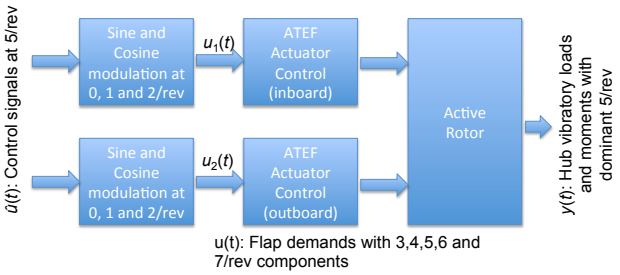

Figure 4: Schematic of the open-loop system.

model of a rotor augmented with ATEF actuators for vibration reduction purposes. The rotor has $N = 5$ blades and two active trailing edge actuators mounted on each blade: inboard ($i = 1$) and outboard ($i = 2$). The rotor behaviour at a given cruise flight condition can be captured by a Linear-Time-Invariant transfer function matrix $G_v(s)$ predicting the effects of N/rev fixed-frame inputs on the N/rev harmonic of the hub loads. The steady-state behaviour at a given rotor speed Ω can be obtained then by the complex matrix $G_v(jN\Omega)$, provided of course that $G_v(s)$ is stable.

We have chosen to perform OBC with 3, 4, 5, 6 and 7/rev harmonics in order to target the 5/rev component of the vibratory hub loads [12]. In order to produce flapping signals at such frequencies, 5/rev fixed-frame control inputs

$$\hat{u}(t) = \begin{bmatrix} \hat{u}_{1,c} \\ \hat{u}_{2,c} \\ \vdots \\ \hat{u}_{10,c} \end{bmatrix} \cos(5\Omega t) + \begin{bmatrix} \hat{u}_{1,s} \\ \hat{u}_{2,s} \\ \vdots \\ \hat{u}_{10,s} \end{bmatrix} \sin(5\Omega t)$$

are modulated with 0, 1 and 2 /rev harmonics as follows

$$\begin{aligned} u_1(t) \;=\; & (\hat{u}_{1,c}\cos(5\Omega t) + \hat{u}_{1,s}\sin(5\Omega t)) + \\ & (\hat{u}_{3,c}\cos(5\Omega t) + \hat{u}_{3,s}\sin(5\Omega t))\cos(\Omega t) + \\ & (\hat{u}_{5,c}\cos(5\Omega t) + \hat{u}_{5,s}\sin(5\Omega t))\sin(\Omega t) + \\ & (\hat{u}_{7,c}\cos(5\Omega t) + \hat{u}_{7,s}\sin(5\Omega t))\cos(2\Omega t) + \\ & (\hat{u}_{9,c}\cos(5\Omega t) + \hat{u}_{9,s}\sin(5\Omega t))\sin(2\Omega t) \end{aligned} \tag{18}$$

$$\begin{aligned} u_2(t) \;=\; & (\hat{u}_{2,c}\cos(5\Omega t) + \hat{u}_{2,s}\sin(5\Omega t)) + \\ & (\hat{u}_{4,c}\cos(5\Omega t) + \hat{u}_{4,s}\sin(5\Omega t))\cos(\Omega t) + \\ & (\hat{u}_{6,c}\cos(5\Omega t) + \hat{u}_{6,s}\sin(5\Omega t))\sin(\Omega t) + \\ & (\hat{u}_{8,c}\cos(5\Omega t) + \hat{u}_{8,s}\sin(5\Omega t))\cos(2\Omega t) + \\ & (\hat{u}_{10,c}\cos(5\Omega t) + \hat{u}_{10,s}\sin(5\Omega t))\sin(2\Omega t) \end{aligned} \tag{19}$$

See Figure 4. The above expressions can be simplified by the use of trigonometric identities to express the flaps as the sum of harmonics 3-7

$$\begin{aligned} u_1(t) &= \sum_{n=3}^{7} (u_{1,c,n}\cos(n\Omega t) + u_{1,s,n}\sin(n\Omega t)) \\ u_2(t) &= \sum_{n=3}^{7} (u_{2,c,n}\cos(n\Omega t) + u_{2,s,n}\sin(n\Omega t)) \end{aligned}$$

A one-to-one linear map from the Fourier coefficients in the fixed frame to those coefficients of the flap signals in the rotating frame can be obtained after solving (18) and (19). For instance, define $\hat{u}_k = [\hat{u}_{1,c}, ..., \hat{u}_{10,c}, \hat{u}_{1,s}, ..., \hat{u}_{10,s}]^T$ and

$$u_k = \begin{bmatrix} u_{1,c,3} \\ \vdots \\ u_{1,c,7} \\ \hline u_{1,s,3} \\ \vdots \\ u_{1,s,7} \\ \hline u_{2,c,3} \\ \vdots \\ u_{2,c,7} \\ \hline u_{2,s,3} \\ \vdots \\ u_{2,s,7} \end{bmatrix}$$

then

$$u_k = X\hat{u}_k \tag{20}$$

where X expressed in (21).

The vibratory response in the frequency domain can thus be expressed in for the considered linear model in the form of (1) with

$$T = \begin{bmatrix} \text{Re}\{G_v(j5\Omega)\} & \text{Im}\{G_v(j5\Omega)\} \\ -\text{Im}\{G_v(j5\Omega)\} & \text{Re}\{G_v(j5\Omega)\} \end{bmatrix} X^{-1}$$

Note that such model representation is possible due to the matrix X being invertible. If the r-th channel of the vibration signal is periodic, it can then be expressed as

$$y_r(t) = y_{r,0} + \sum_{n=1}^{\infty} (y_{r,c,n}\cos(n\Omega t) + y_{r,s,n}\sin(n\Omega t))$$

The output of the frequency domain linear model is expressed by $y_k = [y_{1,c,5}, ..., y_{6,c,5}, y_{1,s,5}, ..., y_{6,s,5},]^T$. Similarly, the upper and lower blocks of the baseline vibration d contain the cosine and sine Fourier coefficients of the 5/rev vibration harmonic with zero flapping, respectively.

(21) $$X = \frac{1}{2}\begin{bmatrix}
0 & 0 & 0 & 0 & 0 & 0 & 1 & 0 & 0 & 0 & 0 & 0 & 0 & 0 & 0 & 0 & 0 & 0 & 1 & 0 \\
0 & 0 & 1 & 0 & 0 & 0 & 0 & 0 & 0 & 0 & 0 & 0 & 0 & 0 & 1 & 0 & 0 & 0 & 0 & 0 \\
2 & 0 & 0 & 0 & 0 & 0 & 0 & 0 & 0 & 0 & 0 & 0 & 0 & 0 & 0 & 0 & 0 & 0 & 0 & 0 \\
0 & 0 & 1 & 0 & 0 & 0 & 0 & 0 & 0 & 0 & 0 & 0 & 0 & 0 & -1 & 0 & 0 & 0 & 0 & 0 \\
0 & 0 & 0 & 0 & 0 & 0 & 1 & 0 & 0 & 0 & 0 & 0 & 0 & 0 & 0 & 0 & 0 & 0 & -1 & 0 \\
0 & 0 & 0 & 0 & 0 & 0 & 0 & 0 & -1 & 0 & 0 & 0 & 0 & 0 & 0 & 0 & 1 & 0 & 0 & 0 \\
0 & 0 & 0 & 0 & -1 & 0 & 0 & 0 & 0 & 0 & 0 & 0 & 1 & 0 & 0 & 0 & 0 & 0 & 0 & 0 \\
0 & 0 & 0 & 0 & 0 & 0 & 0 & 0 & 0 & 0 & 2 & 0 & 0 & 0 & 0 & 0 & 0 & 0 & 0 & 0 \\
0 & 0 & 0 & 0 & 1 & 0 & 0 & 0 & 0 & 0 & 0 & 0 & 1 & 0 & 0 & 0 & 0 & 0 & 0 & 0 \\
0 & 0 & 0 & 0 & 0 & 0 & 0 & 0 & 1 & 0 & 0 & 0 & 0 & 0 & 0 & 0 & 1 & 0 & 0 & 0 \\
0 & 0 & 0 & 0 & 0 & 0 & 0 & 1 & 0 & 0 & 0 & 0 & 0 & 0 & 0 & 0 & 0 & 0 & 0 & 1 \\
0 & 0 & 0 & 1 & 0 & 0 & 0 & 0 & 0 & 0 & 0 & 0 & 0 & 0 & 0 & 1 & 0 & 0 & 0 & 0 \\
0 & 2 & 0 & 0 & 0 & 0 & 0 & 0 & 0 & 0 & 0 & 0 & 0 & 0 & 0 & 0 & 0 & 0 & 0 & 0 \\
0 & 0 & 0 & 1 & 0 & 0 & 0 & 0 & 0 & 0 & 0 & 0 & 0 & 0 & 0 & -1 & 0 & 0 & 0 & 0 \\
0 & 0 & 0 & 0 & 0 & 0 & 0 & 1 & 0 & 0 & 0 & 0 & 0 & 0 & 0 & 0 & 0 & 0 & 0 & -1 \\
0 & 0 & 0 & 0 & 0 & 0 & 0 & 0 & 0 & -1 & 0 & 0 & 0 & 0 & 0 & 0 & 0 & 1 & 0 & 0 \\
0 & 0 & 0 & 0 & 0 & -1 & 0 & 0 & 0 & 0 & 0 & 0 & 0 & 1 & 0 & 0 & 0 & 0 & 0 & 0 \\
0 & 0 & 0 & 0 & 0 & 0 & 0 & 0 & 0 & 0 & 0 & 2 & 0 & 0 & 0 & 0 & 0 & 0 & 0 & 0 \\
0 & 0 & 0 & 0 & 0 & 1 & 0 & 0 & 0 & 0 & 0 & 0 & 0 & 1 & 0 & 0 & 0 & 0 & 0 & 0 \\
0 & 0 & 0 & 0 & 0 & 0 & 0 & 0 & 0 & 1 & 0 & 0 & 0 & 0 & 0 & 0 & 0 & 1 & 0 & 0
\end{bmatrix}$$

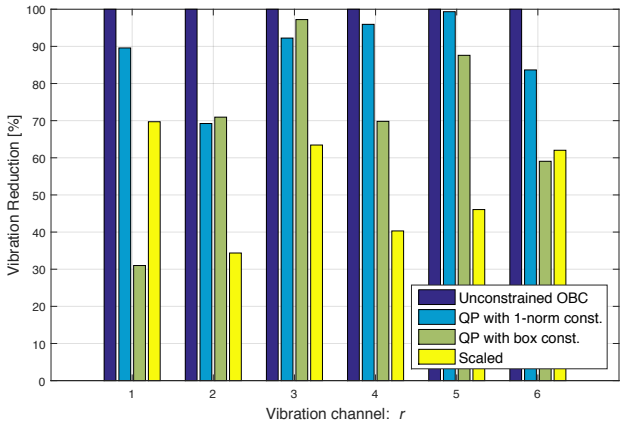

Figure 5: Vibration results with ideal actuation.

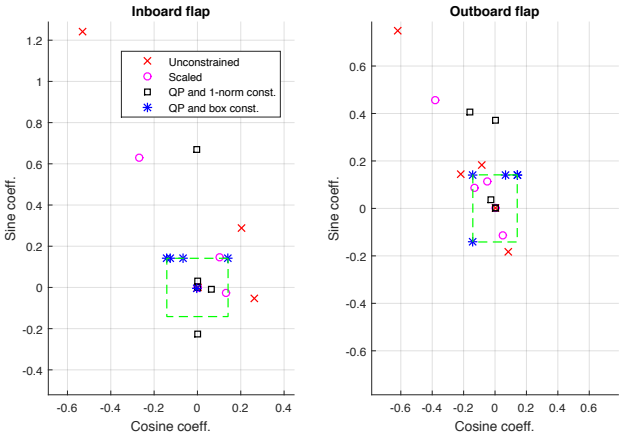

Figure 6: OBC commands.

4.2 Results with Ideal actuation

Firstly, we implement constrained OBC by describing the constrained set using 1-norm constraints (13) and compare them to the more pragmatic approaches of using constrained OBC with box constraints (11) and scaling the solution of unconstrained OBC. The results with ideal actuation are displayed in Figure 5. It is clearly shown the benefits of using refined control algorithms to improve significantly the performance of the control scheme. The average vibration reduction are 88%, 69% and 52.7% for the use of constrained OBC with 1-norm constraints, box constraints description and scaled OBC, respectively. We have chosen $Q = R = I$.

Since five harmonics were chosen to perform the OBC, the reduction ratio for the use of box constraints is $\beta = 1/(5\sqrt{2}) \approx 0.14$. This translates to the QP with box constraints is performed over a feasible space that is five times “smaller” than the one by using 1-norm constraints and for this reason it is more likely to obtain more conservative results. The scaling for scaled OBC was performed by scaling the solution of unconstrained OBC to the largest possible value so the original flap constraints are guaranteed for both actuators. We obtain scaling ratios of about 0.51 and 0.61 for the inboard and outboard flaps, respectively, see Figure 6.

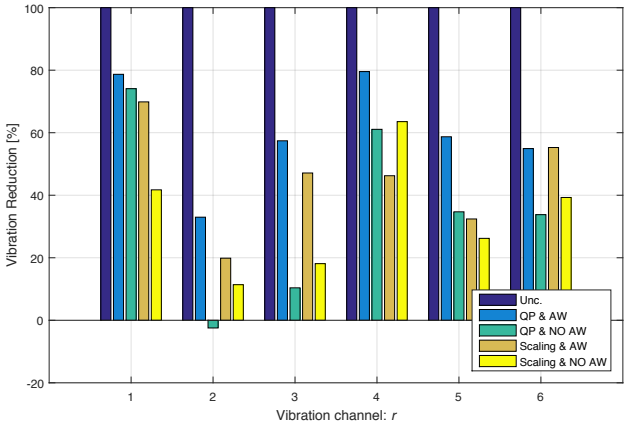

Figure 7: Vibration results taking into account the effects of actuator command saturation.

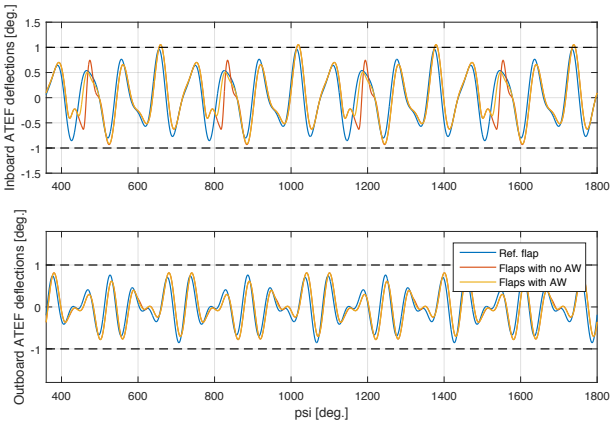

Figure 8: Actuator control system tracking performance. Reference flap demanded by the constrained vibration controller with 1-norm constraints.

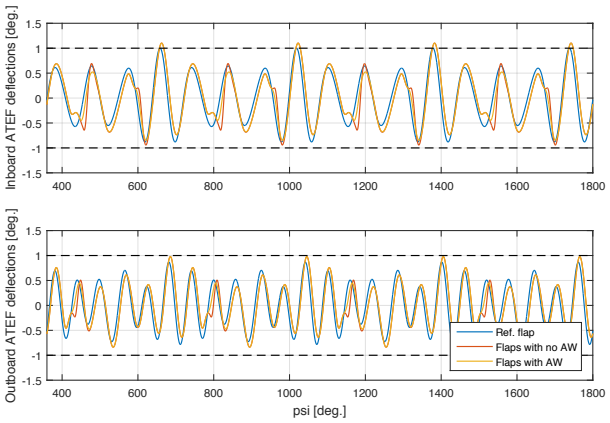

Figure 9: Actuator control system tracking performance. Reference flap demanded by scaled OBC.

4.3 Results with anti-windup actuator compensation

Once we have shown that constrained OBC with 1-norm constraints lead to the least conservative results among the considered OBC practices under ideal actuation assumptions, we focus the attention on the effects of actuator command saturation on such an OBC approach. For comparison purposes, we consider also their effects on the more standard practice of scaled OBC. The general results are shown in Figure 7. Using a combined strategy of constrained OBC with a refined flap constraint description, together with anti-windup actuator compensation, over-performs the standard practice of not using any compensation at all. The average vibration results are about 60.4%, 35.3%, 45.13% and 33.4% for the cases of constrained OBC with anti-windup (QP & AW), constrained OBC without anti-windup (QP & no AW), scaled OBC with anti-windup (Scaling & AW) and scaled OBC without anti-windup (Scaling & No AW), respectively. Both constrained and scaled OBC are shown to be sensitive to the effects of actuator command saturation, with anti-windup compensation offering a performance improvement by about 25% and 12%, respectively. As expected, constrained OBC offer a higher performance and for this reason it is likely to be more sensitive to actuator input saturations, making anti-windup more desirable when this OBC approach is pursued.

The performance of the anti-windup compensator is illustrated in Figures 8 and 9 in the time-domain. For the constrained OBC case, the inboard actuator controller is saturated, while for the scaled OBC, it is the outboard actuator control system the one being saturated. The benefits of anti-windup en each of these situations can be appreciated by the output signal resulting closer to the reference. Such advantages can also be appreciated in the frequency domain, as shown in Figures 10 and 11. The anti-windup compensator, by and large, keep the cosine and sine values closer to the demanded (Ref.) coefficients.

ATEF command signals are restricted to lie in the range [-0.55,0.55] V. The behaviour of the ATEF actuator is modelled similarly to that in [6] by a second-order transfer function

$$G(s) = \frac{k\omega_n^2}{s^2 + 2\zeta\omega_n s + \omega_n^2}$$

with the damping value $\zeta = 0.3$, natural frequency $\omega_n = 377.06$ rad/s and dc-gain $k = 4$. The feedback controller was designed using a $\mathcal{H}_\infty$ mixed-sensitivity control design approach [24], whereby the sensitivity of the actuator closed-loop was shaped in a desired way. The following controller was obtained after the design was performed

$$K(s) \approx \frac{51919(s^2 + 226.2s + 142175)}{(s + 47226)(s + 1346)(s + 0.586)}\,[1, -1]$$

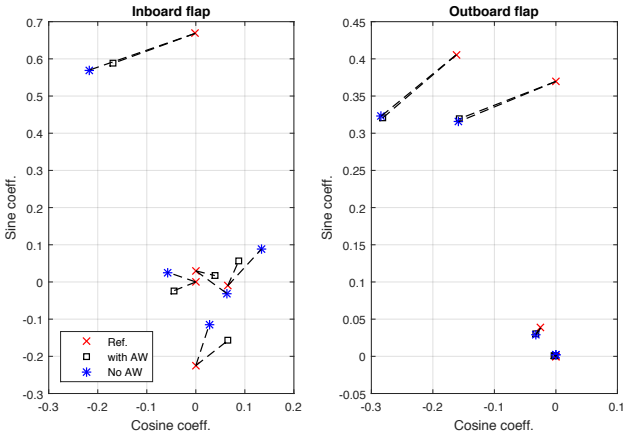

Figure 10: 3-7 harmonic coefficients for constrained OBC using 1-norm constraints with and without anti-windup.

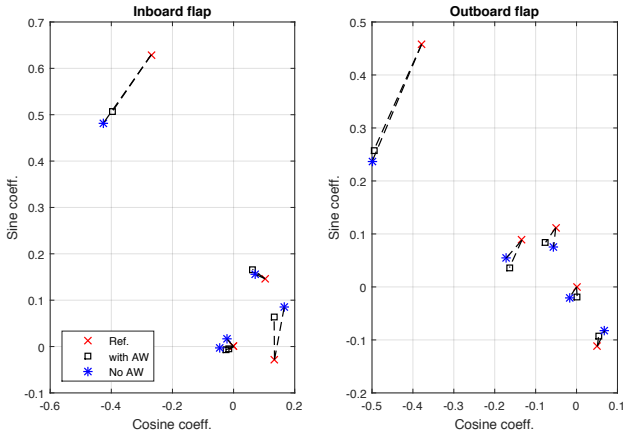

Figure 11: 3-7 harmonic coefficients for scaled OBC with and without anti-windup.

The antiwindup compensator synthesis was performed so robustness properties were given priority: $W_p = 1 \times 10^{-5}$ and $W_r = 0.9$. The obtained value of F is practically zero implying that $M(s) \approx I$. The obtained scheme is the well-known anti-windup compensator scheme known as *IMC anti-windup* [30], which is known to offer the same robustness characteristics against unstructured uncertainty of the unconstrained actuator control loop [27, 16].

5 CONCLUDING REMARKS

This work has combined for the first time two types of constraint handling techniques to improve the performance of OBC systems targeting vibration alleviation. Flap constraints are handled by incorporating constrained optimisation techniques in the design of the top-level vibration controller. Actuator command restrictions can have a significant deteriorating effect on the overall performance and they are handled in this work using anti-windup compensation techniques. The combination of both constraint handling methods can offer significant advantages with respect to the use of more pragmatic approaches (the average reduction level across the vibration channels in the considered simulation example was improved by a factor of 2 approximately).

In cases where actuator command saturations are not important, the performance can be definitely improved by using constrained OBC with respect to pragmatic uses of unconstrained OBC. The use of refined descriptions for the flap constraints under a QP framework can also offer significant benefits in enhancing the performance, but these should be considered with care as they could introduce an additional computational burden in real applications. In addition, constrained OBC with refined descriptions can be at a higher risk to saturate the actuator as the produced reference flaps can be larger in magnitude. In such scenarios the performance could end up being about the same, if not worse, than constrained OBC with less refined constraint set descriptions, but which are easier to implement. If actuator is expected to become saturated, anti-windup compensation techniques are likely to offer the benefits to avoid a major performance deterioration with either constrained or unconstrained OBC. In any situation, both constraint handling methods have their limitations and performance degradation can be unavoidable. Ultimately, it is the control designer's duty to investigate a priori if such design refinements for flap and command input constraints are worth the effort depending on the specific application.

ACKNOWLEDGEMENTS

The authors would like to thank Peter Court (AgustaWestland, UK) and Chris Hutchin (Defence Science and Technology Laboratory (DSTL), UK), for some useful discussions in certain technical aspects of this work.

COPYRIGHT STATEMENT

as part of the ERF 2015 proceedings or as individual off-prints from the proceedings.

References

[1] E. Ahci and R. Pfaller. Structural design, optimization and validation of the integrated active trailing edge for a helicopter rotor blade. In *Proceedings of the 64th American Helicopter Society Forum*, Montreal, Canada, 2008.

[2] K. Åström and B. Wittenmark. *Adaptive Control*. Dover Publications, 2008.

[3] M. Bebesel, D. Roth, and R. Pongratz. Reduction of BVI on ground – Inflight evaluation of closed-loop controller. In *Proceedings of the 28th European Rotorcraft Forum*, Montreal, Canada, 2002.

[4] S. Boyd, L. E. Ghaoui, E. Feron, and V. Balakrishnan. *Linear Matrix Inequalities in Systems and Control Theory*. SIAM: Studies in applied mathematics, 1994.

[5] S. Boyd and L. Vandenberghe. *Convex Optimization*. Cambridge university press, 2004.

[6] L. R. Centolanza, E. C. Smith, and B. Munsky. Induced-shear piezoelectric actuators for rotor blade trailing edge flaps. *Smart Materials and Structures*, 11(1):24–35, 2002.

[7] S. J. Elliott. *Signal Processing for Active Control*. Academic Press, 2001.

[8] P. P. Friedmann. On-blade control of rotor vibration, noise and performance: Just around the corner? *American Helicopter Society Journal*, 59:041001 (1–37), 2014.

[9] P. P. Friedmann and A. K. Padthe. Vibration and noise alleviation in rotorcraft using on-blade control implemented by microflaps. In *Proceedings of the 38th European Rotorcraft Forum*, Amsterdam, Netherlands, 2012.

[10] R. B. Green, E. A. Gillies, and Y. Wang. Trailing edge flap flow control for dynamic stall. *The Aeronautical Journal*, 115(1170):493–503, 2011.

[11] W. Johnson. Self-tuning regulators for multicyclic control of helicopter vibration. Technical report, NASA, 1982.

[12] W. Johnson. *Helicopter Theory*. Dover Publications, 1994.

[13] H. K. Khalil. *Nonlinear Systems (third edition)*. Prentice Hall, Upper Saddle River, 2002.

[14] J-S. Kim, K. W. Wang, and E. C. Smith. Development of a resonant trailing-edge flap actuation system for helicopter rotor vibration control. *Smart Materials and Structures*, 16(6):2275 – 2285, 2007.

[15] R. M. Morales. Alternative representations of frequency-domain constraints for improved performance in on-blade control systems. In *54th IEEE Conference on Decision and Control*, Osaka, Japan, 2015. Under revision.

[16] R. M. Morales, G. Li, and W. Heath. Anti-windup and the preservation of robustness against structured norm-bounded uncertainty. *International Journal of Robust and Nonlinear Control*, 24(17):2640–2652, 2014.

[17] R. M. Morales and M. C. Turner. Control design and assessment of active trailing edge actuators for a rotor model. In *Proceedings of the 69th American Helicopter Society Forum*, Phoenix, USA, 2013.

[18] R. M. Morales and M. C. Turner. Robust anti-windup design for active trailing edge flaps in active rotor applications. In *Proceedings of the 70th American Helicopter Society Forum*, Montreal, Canada, 2014.

[19] R. M. Morales, M. C. Turner, P. Court, and C. Hutchin. Actuator constraints handling in higher harmonic control algorithms for vibration reduction. Southampton, UK, 2014. Proceedings of the 40th European Rotorcraft Forum.

[20] D. Patt, L. Liu, J. Chandrasekar, D. S. Bernstein, and P. P. Friedmann. HHC algorithm for helicopter vibration reduction revisited. *Journal of Guidance, Control and Dynamics*, 28(5):918 – 930, 2005.

[21] A. Rabourdin, J. Maurice, O. Dieterich, and P. Konstanzer. Blue pulse active rotor control at airbus helicopters—New EC145 demon- strator and flight test results,. In *Proceedings of the 70th American Helicopter Society Forum*, Montreal, Canada, 2014.

[22] K. Ravichandran, I. Chopra, B. Wake, and B. Hein. Trailing-edge flaps for rotor performance enhancement and vibration reduction. *Journal of the American Helicopter Society*, 58(2):1–13(13), 2013.

[23] D. Roth. Advanced vibration reduction by IBC technology. In *Proceedings of the 30th European Rotorcraft Forum*, Maastricht, The Netherlands, 2004.

[24] S. Skogestad and I. Postlethwaite. *Multivariable Feedback Control: Analysis and Design (second edition)*. John Wiley & Sons, 2005.

[25] F. K. Straub, V. Anand, T. S. Birchette, and B. H. Lau. Wind tunnel test of the SMART active flap rotor. In *Proceedings of the 65th American Helicopter Society Forum*, Grapevine, USA, 2009.

[26] S. Tarbouriech, G. Garcia, J. Gomes da Silva Jr., and I. Queinnec. *Stability and stabilization of linear systems with saturating actuators*. Springer, 2011.

[27] M. C. Turner, G. Herrmann, and I. Postlethwaite. Incorporating robustness requirements into antiwindup design. *IEEE Transactions on Automatic Control*, 52(10):1842–1855, 2007.

[28] P. F. Weston and I. Postlethwaite. Linear conditioning for systems containing saturating actuators. *Automatica*, 36:1347 – 1354, 2000.

[29] L. Zaccarian and A. Teel. *Modern Anti-windup Synthesis*. Princeton University Press, 2011.

[30] A. Zheng, M. V. Kothare, and M. Morari. Antiwindup design for internal model control. *International Journal of Control*, 60(5):1015–1024, 1994.